Geobios 90 (2025) 17–30

Contents lists available at ScienceDirect

Geobios

journal homepage: www.elsevier.com/locate/geobio

Research Paper

Micro-CT reconstruction reveals new information about the phylogenetic position and locomotion of the Early Cretaceous bird *Iberomesornis romerali* ☆

Javier Castro-Terol [a], Alejandro Pérez-Ramos [a], Jingmai K. O'Connor [b], José Luis Sanz [c], Francisco J. Serrano [a,d,*]

[a] Department of Ecology and Geology, University of Málaga 29070 Málaga, Spain
[b] Negaunee Integrative Research Center, Field Museum of Natural History, Chicago, IL 60605, USA
[c] Real Academia de Ciencias Exactas, Físicas y Naturales, 28004 Madrid, Spain
[d] Dinosaur Institute, Natural History Museum of Los Angeles County, 90007 California, USA

ARTICLE INFO

Article history:
Received 13 March 2024
Revised 21 November 2024
Accepted 28 November 2024
Available online 5 March 2025

Keywords:
Enantiornithes
Mesozoic birds
Avian evolution
Computed tomography scanning
Bone reconstruction
Flight mechanics
Las Hoyas

ABSTRACT

The enantiornithine *Iberomesornis romerali* from the Lower Cretaceous site of Las Hoyas (Spain) was originally described more than 35 years ago. As one of the first known articulated partial skeletons of this clade, *I. romerali* has been critical to our understanding of early avian systematics. Due to its preservation as a largely two-dimensional slab specimen, previous anatomical descriptions were unable to fully capture its anatomy. Here, we present new anatomical data based on micro-computed tomography of the holotype. We reconstruct five previously poorly known osteological elements, i.e., cervical vertebrae, pygostyle, coracoid, furcula, and humerus. Re-evaluation of these elements resulted in revised scorings for 15 morphological characters commonly used for cladistic analysis of Aves. The results of the modified character matrix support *Iberomesornis* in a derived position within Enantiornithes, close to the Longipterygidae. In addition, new findings in the coracoid and humerus reveal well-developed muscles for the elevation (i.e., supracoracoideus) and flexion–extension (extensor carpi radiale) of the wing. The new evidences, together with the typical enantiornithine furcula and the small size of the holotype, suggest that *I. romerali* was capable of flapping flight.

1. Introduction

Enantiornithes were the most speciose lineage of Cretaceous birds with fossils found on all continents, except Antarctica (O'Connor et al., 2011; O'Connor, 2022). Our knowledge about the diversity of this group has substantially increased in the last two decades due to the huge number of fossils unearthed, particularly from the Lower Cretaceous deposits at northeastern China (Chiappe and Meng, 2016; O'Connor, 2022).

The lacustrine Lagerstätte of Las Hoyas from La Huerguina Fm. in central Spain (ca. 129–126 Ma; Fig. 1) is the most exceptional source of Cretaceous birds in Europe. All collected specimens are referable to Enantiornithes; cumulatively these fossils provide key information regarding phylogeny, ecology, locomotion, and life history of this clade (Sanz et al., 1988, 1996, 2002; Sanz and Buscalioni, 1992; Navalón et al., 2015; Poyato-Ariza and Buscalioni, 2016; Knoll et al., 2018; Serrano et al., 2018; Cubo et al., 2022; Nebreda et al., 2023). Particularly, the 'unusual' Early Cretaceous bird *Iberomesornis romerali* was described thirty-six years ago (Sanz et al., 1988), when only a few fossils of Cretaceous birds were known globally. The generic epithet *Iberomesornis* (meaning Iberian intermediate bird) referred to its place of origin and preserved anatomical features that were intermediate between *Archaeopteryx* and ornithurines known at that time (e.g., *Ichthyornis* and *Hesperornis*; Sanz et al., 1988). Subsequent cladistic analyses that grew in scale as they successively incorporated new discoveries (e.g., *Sinornis*, *Concornis*, *Patagopteryx*, *Confuciusornis*) supported the inclusion of *I. romerali* into the clades Pygostylia, Ornithothoraces and Enantiornithes, based on the presence of a proportionately large pygostyle (Pygostylia), a strut-like coracoid (Ornithothoraces), a Y-shaped furcula with long hypocleidium, a humerus with distal condyles transversely oriented, a round articular surface of the proximal tibiotarsus, and partial fusion of the tarsometatarsus (Enantiornithes) (Kurochkin, 1985; Sanz and

☆ Corresponding editor: Antoine Louchart.
* Corresponding author.
E-mail address: fjsa@uma.es (F.J. Serrano), fjsa@uma.es (F.J. Serrano).

https://doi.org/10.1016/j.geobios.2024.11.006
0016-6995/

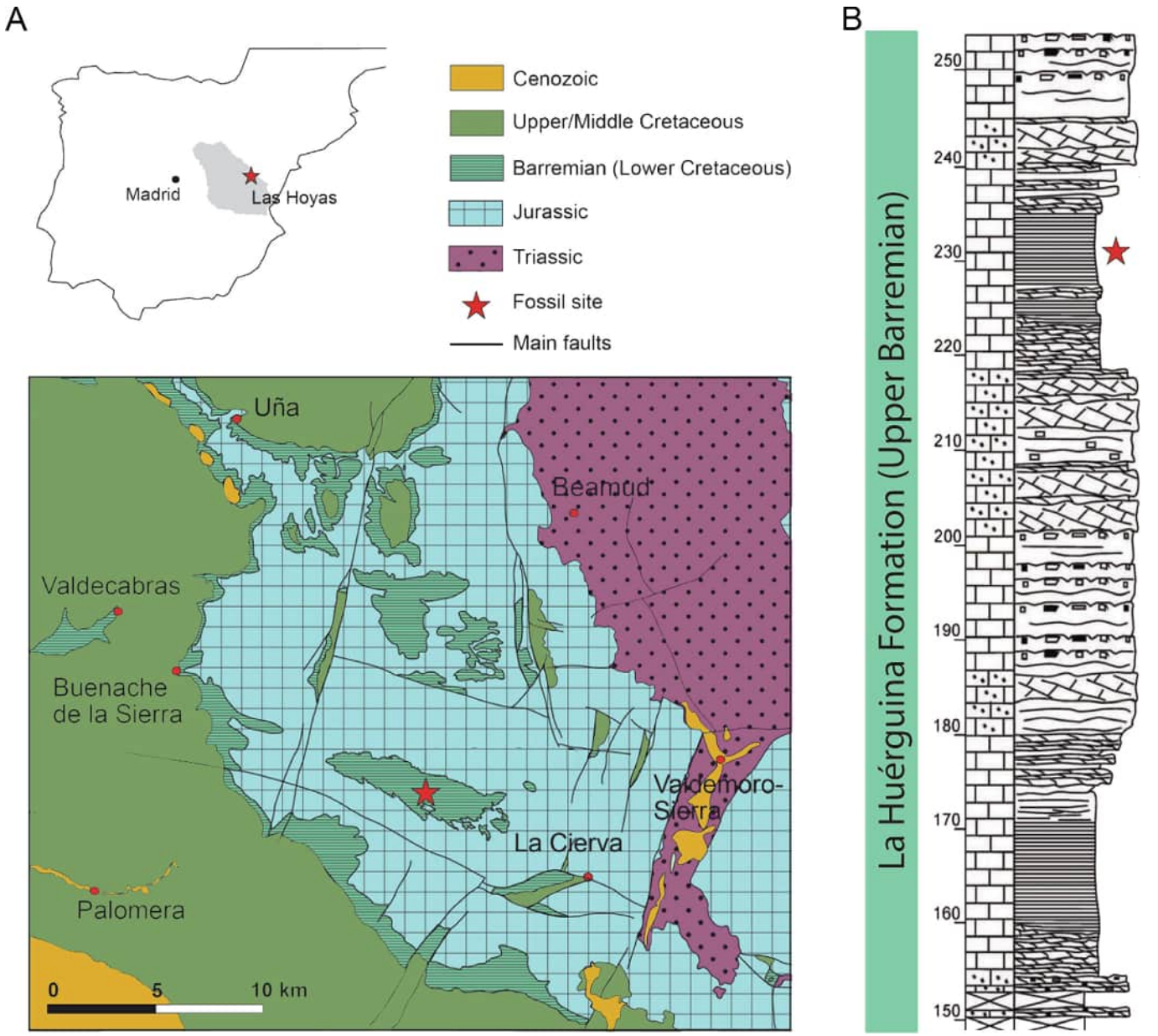

Fig. 1. A. Geographical location and geological information of Las Hoyas fossil site in the Iberian Peninsula. **B.** Chronostratigraphic position of the fossil site. Images taken and modified from Fregenal-Martínez et al. (2017) and Marugán-Lobón et al. (2023), with permission of the authors.

Buscalioni, 1992; Sereno, 2000; Chiappe, 2002). More recent analyses including a much higher number of Cretaceous avian taxa differ with regards to the relative position of *Iberomesornis* within Enantiornithes: embedded in an enantiornithine polytomy (O'Connor et al., 2011); basal and closest to *Protopteryx* (Atterholt et al., 2018); or more derived and closer to Longipterygidae (O'Connor and Zhou, 2013; Wang et al., 2022b).

The last anatomical studies describing the holotype of *I. romerali* were published more than 20 years ago (Sereno, 2000; Sanz et al., 2002). Like many other fossil birds preserved in slabs, the skeleton is two-dimensionally preserved and crushed, and many characters could not be observed originally due to its preservation in a slab which leaves a considerable portion of the skeleton hidden in the matrix. As a result, many potentially informative characters regarding the phylogenetic position of *Iberomesornis* could not be assessed.

Recent research concerning the functional morphology and flight abilities of enantiornithines suggest they were able to fly similarly to many modern birds and most likely utilized some form of intermittent flight (Close and Rayfield, 2012; Feo et al., 2015; Liu et al., 2017, 2019; Serrano et al., 2018; Chiappe et al., 2020; Pei et al., 2020). However, some studies suggest that the unusual shoulder configuration in these birds would have limited wing movement, resulting in a unique mechanics of flight different from that present in extant birds (Mayr, 2017; Wang et al., 2022a). In order to shed light on the flight performance of Enantiornithes and other early birds, the 3D morphology and reconstruction of the wing and pectoral girdle bones is required.

The application of computed tomography (CT) scanning has greatly increased our capacity to assess fossil morphology by virtually extracting the skeleton from the rock for 3D visualization and assessing internal structures (Knoll et al., 2018; Voeten et al., 2018;

Wang et al., 2022a). In the present study we reanalyze the holotype of *I. romerali* using micro-CT based segmentation and 3D reconstruction. We focus on five osteological structures, two from the axial skeleton (i.e., cervical vertebrae and pygostyle) and three from the appendicular skeleton (i.e., coracoid, furcula and humerus). These parts were best preserved and had most potential to reveal new information regarding phylogeny and flight of *Iberomesornis*. Other more delicate and crushed areas, which will require much more work (and may not even reveal information) will be the subject of a separate study.

2. Material and methods

2.1. Fossil holotype

Iberomesornis romerali, LH-22, is housed in Museo Paleontológico de Castilla-La Mancha (MUPA), Cuenca, Spain. It was found in Las Hoyas, a fossil site from the Calizas de La Huérguina Fm., dated to the Late Barremian of the Lower Cretaceous (Fregenal-Martínez et al., 2017; Sanz et al., 2002; Fig. 1). LH-22 is a nearly complete articulated specimen preserved in lithographic limestone resting on its right side (Fig. 2), lacking the skull, cranial cervical vertebrae, most of the sternum and hands, as well as soft tissues. In addition, it is worth noting that this fossil lacks preserved soft tissues. The specimen is relatively well preserved but erosion, crushing, and local displacement are observable. High-resolution images of the fossil were obtained using a macro lens (Canon EOS EF 50 mm F/1.8) of a camera Canon EOS 6D. The terminology regarding anatomy primarily follows Baumel et al. (1993), and also Sereno (2000), Panteleev (2018), and Wang et al. (2022a).

2.2. Micro-CT data acquisition, processing, and three-dimensional reconstruction

The holotype was scanned by the SkyScan 2214 located in Servicios Centrales de Apoyo a la Investigación at Universidad de Málaga, Spain. The fossil was put inside a polystyrene structure to allow a correct positioning in the scanner. After modifying a number of parameters for the scanner (Table 1), we obtained a scan consisting of 4297 slices at a voxel size of 21.5 µm. We applied contrast correction filters to the raw micro-CT data using *Fiji* software v.2.21.0 (Schindelin et al., 2012) to improve the visualization of the images by decreasing the artifacts produced during the data acquisition process (Pérez-Ramos and Figueirido, 2020). Segmentation of five osteological structures, namely, cervical vertebrae, left coracoid, furcula, left humerus, and pygostyle was performed using *Avizo* software v.7.1 (https://www.vsg3d.com) to generate different virtual layers separating different bones (thresholding), calibrating histogram ranges – which are directly related to palaeohistological and taphonomical characteristics –, and selecting region of interest (ROIs). The volume of each layer was inferred by means of voxel size interpolations and the bones were virtually extracted with their measurements exactly matching the original ones (Grau, 2003; Abel et al., 2012; Sutton et al., 2014; Pérez-Ramos and Figueirido, 2020).

Virtual model bones corresponding to the (*i*) cervical vertebrae, (*ii*) pygostyle, (*iii*) coracoids, (*iv*) furcular, and (*v*) left humerus of LH-22 were generated using *Geomagic Studio* 2013 software (https://www.3dsystems.com). Remeshing techniques like smoothing and noise reduction were applied on these models in order to remove artifacts generated during the scanning or segmentation processes (Grau, 2003; Pérez-Ramos and Figueirido, 2020). Bones were mirrored due to the inversion of the CT data with respect to the fossil, and then reoriented so that the Z-axis coincided with the exposed region of the fossil in the rock. The Z-axis thus corresponds to the plane in which the bones were crushed. In addition, the missing parts of the pygostyle were reconstructed according to the cast outline discernible from the rock. In the case of the furcula, the position of some parts of the bone (i.e., broken or dislocated parts) were manually repositioned in the correct anatomical position. CT images of this bone allowed to discern between areas of high- and low-density (Fig. S1, Appendix A), because the interaction with X-rays is higher in the denser zones. High-density bone zones (distributed along the posteromedial margin of the rami and the dorsoventral axis of the hypocleidium) were interpreted as collapsed bone walls, and thereafter reconstructed as elevated areas in the 3D virtual model.

2.3. Phylogenetic analysis

We amended the scoring of 15 previously hidden characters for *Iberomesornis* in Atterholt et al.'s (2018) character matrix. These pertain to new information gleaned from the cervical vertebrae, pygostyle, coracoid, furcula, and humerus (Table 2). Almost all these new scorings are replacing missing information. Scorings for two fusion characters were also changed based on the comparison with other enantiornithines that suggests the lack of fusion in the compound bones of the hindlimb reflects immaturity and that these bones would most likely fuse with maturity (Hu and O'Connor, 2017).

The basal enantiornithine *Protopteryx* was also added, resulting in a matrix with 47 operational taxonomic units (OTU) scored across 252 characters. The matrix was analyzed using the software TNT (Goloboff and Morales, 2023) with memory set to 10,000 trees. We conducted a heuristic search saving the shortest tree out of every 1,000 trees followed by a second round of tree-bisection reconnection (TBR). The first round of TBR produced 12 trees 936 steps long. The second round of TBR produced 2321 trees of the same length. We also ran the analysis without *Protopteryx* (46 OTU), resulting in a single tree 923 steps long in the first round of TBR and 78 trees in the second round of TBR.

3. Results

Micro-CT data allowed the reconstruction of five osteological structures from the holotype of *Iberomesornis romerali*, two from the axial skeleton (cervical vertebrae and pygostyle) and three from the appendicular skeleton (coracoid, furcula, and humerus) (Fig. 2). New anatomical and morphological findings relevant for systematics are described and compared to previous observations in the following sections. The new rescored characters (Table 2) were incorporated to the matrix to perform the phylogenetic analyses.

3.1. Cervical vertebrae

Iberomesornis romerali preserves the five caudalmost vertebrae in the cervical series, although the most proximal of these is only a small fragment (Fig. 3(A)); the rest are well-preserved and complete. Of these four, the two cranialmost cervicals (i.e., 'a' and 'b'; Fig. 3) are elongated and have a lateral shelf connecting the prezygapohysis and the postzygapophysis, with the latter being long and curved with a low epipophysis, as observed by Sereno (2000) and Sanz et al. (2002). The postzygapophysis of the next preserved cervical (i.e., 'c') is remarkably arched (Fig. 3(B–D)), reminiscent of those X-shaped cervicals observed in *Parabohiaornis martini* (Wang, 2023). These three cervicals lack spinous processes, which were reported present in the last preserved cervical (i.e., 'd') (Sereno, 2000; Sanz et al., 2002), but cannot be confirmed in our micro-CT data. Preservation of the parapophysis in 'b' and

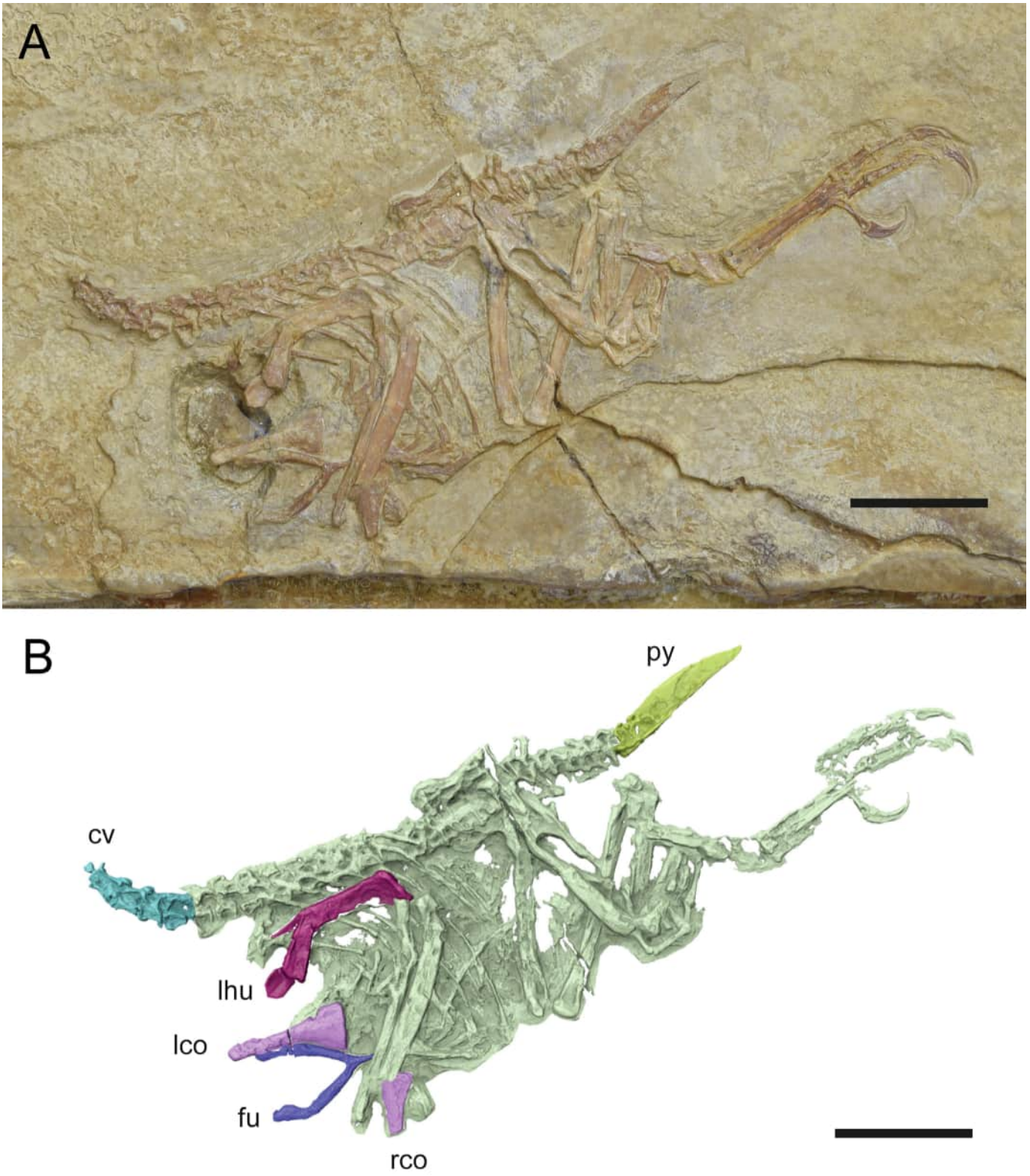

Fig. 2. Holotype of *Iberomesornis romerali* LH-22 from the paleontological collection of MUPA. **A.** Fossil on its lithographic plate from the Las Hoyas site, Spain. **B.** Virtual model of *I. romerali* obtained from a micro-CT scan at the University of Malaga. Anatomical elements highlighted in color indicate the osteological structures analyzed in the present study. Abbreviations: cv, cervical vertebrae; lco, left coracoid; fu, furcula; hu, humerus; py, pygostyle; rco, right coracoid. Scale bars: 1 cm.

diapophyses in 'b', 'c' and 'd' – although broken – suggests the presence of partially fused cervical ribs (Sanz and Bonaparte, 1992; Sereno, 2000). The centra of the two caudalmost preserved cervical vertebrae ('c' and 'd') are laterally excavated and with keeled ventral surfaces, which are developed into a cranially positioned hypapophysis in the latter. Ventrally keeled centra are reported in

Table 1
Values of the main acquisition parameters programmed in the scanner to obtain the CT data.

Source Voltage (kV)	125.00
Source Current (μA)	104.00
Source Target Power (W)	12.11
Image Pixel Size (μm)	21.50
Scan duration	10 h:21 min:33 s
Rotation Step (deg)	0.010

Table 2
Scoring of the changed characters in order to respect the matrix of Atterholt et al. (2018).

Character #	Character and states description	Character state changed
50	One or more pneumatic foramina piercing the centra of mid cranial cervicals caudal to the level of the parapophysis-diapophysis: present (0); absent (1).	? to 0
52	Prominent carotid processes in the intermediate cervicals: absent (0); present (1).	? to 1
76	Cranial end of pygostyle dorsally forked: absent (0); present (1).	? to 1
77	Cranial end of pygostyle with a pair of laminar, ventrally projected processes: absent (0); present (1).	? to 1
78	Distal constriction of pygostyle: absent (0); present (1). In the pygostyles of some enantiornithine taxa, the distalmost mediolateral width is reduced so that the midline of the pygostyle projects distally farther than the lateral margins (Chiappe et al. 2002).	? to 1
84	Scapula: articulated at the shoulder end of the coracoid (0); well below it (1).	? to 1
85	Coracoid, humeral articular facet: dorsal to acrocoracoid process (0); ventral to acrocoracoid process (1).	? to 0
88	Laterally compressed shoulder end of the coracoid with nearly aligned acrocoracoid process, humeral articular surface, and scapular facet in dorsal view: absent (0); present (1).	? to 1
93	Coracoid, medial surface, strongly depressed elongate furrow at the level of the passage of the n. supracoracoideus: absent (0); present (1).	? to 1
106	Dorsal and ventral margins of the furcula: sub equal in width (0); ventral margin distinctly wider than the dorsal margin so that the furcula ramus appears concave laterally (1).	? to 1
107	Hypocleidium: absent (0); present as a tubercle or short process (1); present as an elongate process approximately 30% rami length (2); hypertrophied exceeding 50% rami length (3).	[23] to 2
136	Well-developed olecranon fossa on the caudal face of the distal end of the humerus: absent (0); present (1).	? to 1
142	Humerus, distal condyles: subround, bulbous (0); weakly defined, "straplike" (1).	? to 1
209	Tibia, calcaneum, and astragalus: unfused or poorly co-ossified (sutures still visible) (0); complete fusion of tibia, calcaneum, and astragalus (1).	0 to 1
222	Metatarsals II-IV, intermetatarsal fusion: absent or minimal co-ossification (0); partial fusion (sutural contacts easily discernible) (1); completely (or nearly completely) fused (sutural contacts absent or poorly demarcated) (2).	0 to 1

several Early Cretaceous enantiornithines – e.g., *Concornis lacustris* (Sanz et al., 2002), *Sulcavis geeorum* (O'Connor et al., 2013), *Piscivorenantiornis inusitatus* (Wang and Zhou, 2020), and *Parabohaiornis martini* (Wang, 2023). Raw micro-CT data and the reconstructed models reveal the presence of a small but prominent carotid process in the second preserved cervical (revised scoring for character 52), reminiscent of those of *Sulcavis geeorum* (O'Connor et al., 2013), as well as a pneumatic foramen piercing the centrum at the level of the diapophysis in the caudal region of the first complete, preserved cervical (revised scoring for character 50; Fig. 3 (B, D)), a structure also reported in more stem birds like *Archaeopteryx* (Britt et al., 1998).

3.2. Pygostyle

LH-22 presents eight free caudal vertebrae that articulate distally with the pygostyle, which is moderately well-preserved proximally but distally only preserves the ventral portion (Fig. 4). The first three caudals contributing to the pygostyle can be delimited, indicating that the fusion bone is incomplete. Micro-CT data reveals that cranially, the pygostyle has two proximoventral processes preserved: one bulky and laterally projected, and another more pointed and proximally projected (Fig. 4(C)). We tentatively identified them as the left and right proximoventral processes due to its position as a symmetrically bilateral structure; by assuming that their differences in size and shape result from the deformation affecting the bone. In addition, the left ventrolateral ridge longitudinally extended (from the cranial to the caudal region) and laterally projected is observed. Distally, the mediolateral width is constricted so that the midline of the pygostyle projects distally farther than the lateral margins. These features are found commonly in other enantiornithines (Chiappe and Walker, 2002; Chiappe et al., 2002; Wang and O'Connor, 2017); Atterholt et al., 2018). From these observations, scoring for characters 76, 77 and 78 were revised (Table 2).

3.3. Coracoid

The two coracoids of *I. romerali* LH-22 are exposed in ventral view (Fig. 2). The morphology is typically enantiornithine, that is, strut-like with a conspicuous head followed by a shaft that distally expands forming the triangular pterygoma (Fig. 5(A)). The shaft is relatively similar in length to the head (shaft elongates in some taxa, e.g., *Enantiornis* and *Neuquenornis*; O'Connor, 2009). Lateral and medial margins of the pterygoma are nearly straight – in contrast with some other enantiornithines in which the lateral margin is strongly convex (e.g., *Concornis* or *Eoalulavis*) – with only a slight convexity of the lateral margin distally near to the broad and straight sternal margin (Sanz et al., 1988; Sereno, 2000; Chiappe and Witmer, 2002).

The right coracoid only preserves the distal half, with the medial pterygoma underlying the distal ulna. Micro-CT images of the right coracoid revealed that the covered portion is poorly preserved (Fig. S2, Appendix A). The reconstruction presented here relies on the almost complete left coracoid. Micro-CT data reveals the morphology of the dorsal surface (Fig. 5). The distal end of the coracoid has a poorly developed, blunt acrocoracoid process that is rounded in the ventral face and proximodistally aligned with the humeral and scapular articular facets in dorsal view (Fig. 5(B, C)), as typical in Enantiornithes (Zhang et al., 2014; Atterholt et al., 2018; Panteleev, 2018). In the ventral face, at least one lateral ridge of the acrocoracoid is observed expanding from the top of the acrocoracoid process to the humeral articular surface (Fig. 5(B)). The dorsal surface of the acrocoracoid process appears to be eroded so that it appears concave. The scapular facet is angled proximally (it forms a 76.5° angle with the long axis of the shaft) and the articular surface of this facet is remarkably concave (Fig. 5(C)). In enantiornithines, the surface of this facet is flat to weakly convex, opposed to the concave facet presented by ornithuromorphs (Chiappe, 2002; Panteleev, 2018; O'Connor, 2022; Wang et al., 2022a). The clear concave facet reported here

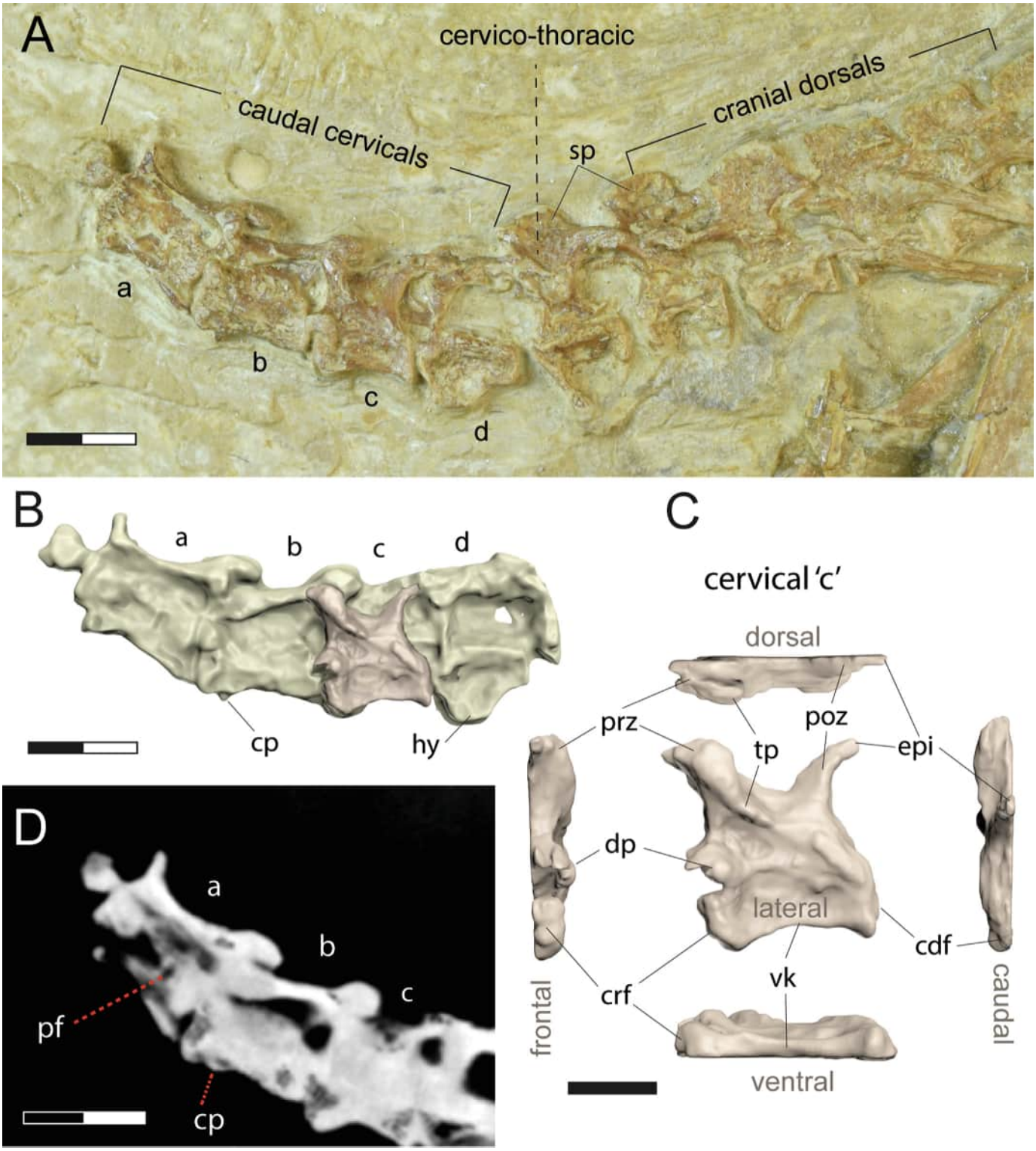

Fig. 3. Cervical vertebrae of *Iberomesornis romerali*. **A.** Original fossil (holotype, LH-22). **B.** Virtual model segmented from micro-CT scan of the four posteriormost cervicals. **C.** Detailed virtual model of the second last posterior cervical. **D.** Micro-CT slice of three most anterior cervicals preserved. Abbreviations: cdf, caudal articular facet of centrum; cp, carotid process; crf, cranial articular facet of centrum; dp, diapophysis (broken); epi, epipophysis; hy, hypapophysis; pf, pneumatic foramina; poz, postzygapophysis; prz, prezygapophysis; sp, spinous process; tp, tranverse process; vk, ventral keel. Scale bars: 2 mm (A, B, D), 1 mm (C).

in *I. romerali* could be attributed thus to (*i*) an independent development of an ornithuromoph-like facet in this enantiornithine, or most likely (*ii*) to the fact that the deformation/crushing of the bone has exaggerated the concavity from an original flatter surface. Considering these two possibilities, this character was not included in the matrix for phylogenetic analysis.

The dorsal surface of the shaft is concave, and the medial margin seems thicker than the lateral one, forming a prominent medial

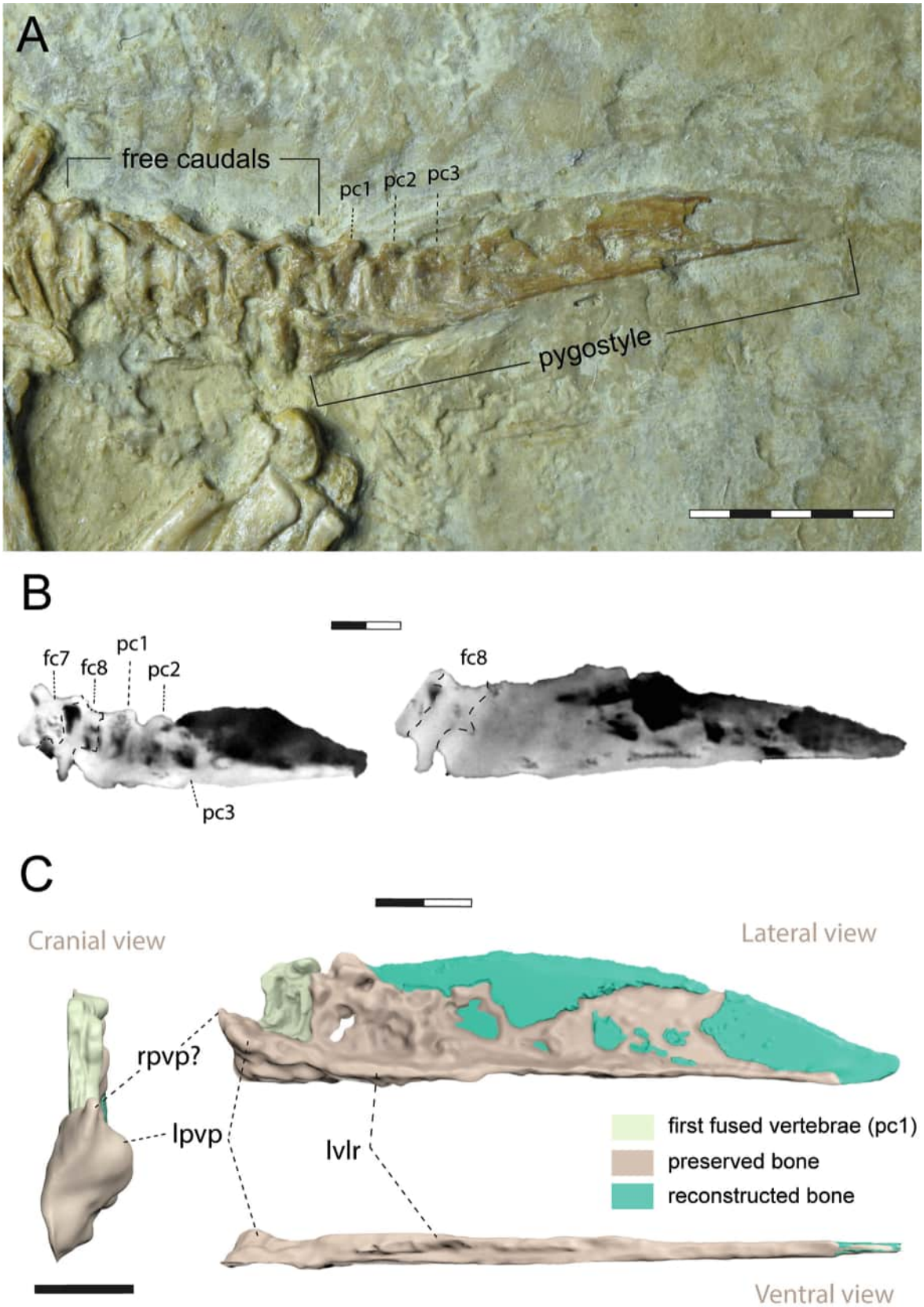

Fig. 4. Pygostyle of *Iberomesornis romerali*. **A.** Original fossil (holotype, LH-22). **B.** Micro-CT slices in laterocaudal and lateral views. **C.** Virtual model segmented from micro-CT scan. Abbreviations: fc, free caudal vertebrae; lvlr, left ventrolateral ridge; pc, caudal vertebrae fused to pygostyle; rpvp, right proximoventral process; lpvp, left proximoventral process. Scale bars: 5 mm (A), 2 mm (B, C), 1 mm (C).

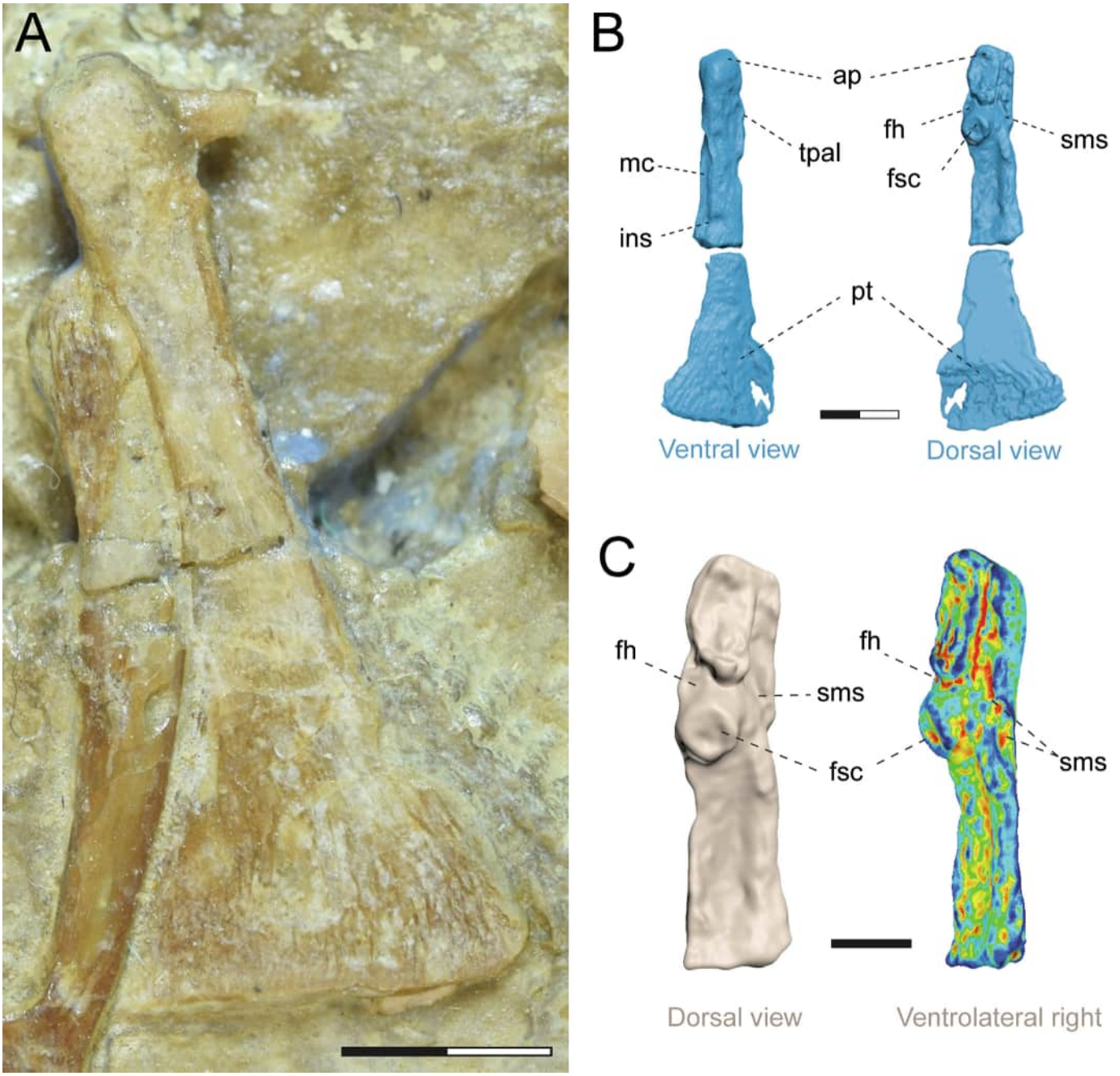

Fig. 5. Left coracoid of *Iberomesornis romerali*. **A.** Original fossil (holotype, LH-22), ventral view. **B.** Virtual model segmented from micro-CT scan. **C.** Reconstructed model of distal coracoid (left) applying a curvature filter to highlight the grooves and anatomical marks (right). Abbreviations: ap, acrocoracoid process; mc, medial crest (scapular wing); fh, humeral facet (glenoid); fsc, scapular facet; ins, supracoracoid nerve incisure; pt, pterygome (sternal wing); sms, supracoracoid groove; tpal, acrocoracoid ridge. Scale bars: 2 mm (A, B), 1 mm (C).

crest that was originally hidden under the left furcular ramus (Fig. 5(A, B)). These features are similar to the Early Cretaceous *Piscivorenantiornis* (Wang et al., 2022a) and the Late Cretaceous enantiornithines from Dzharakuduk locality of the Bissetky Fm., Uzbekistan (Panteleev, 2018). The preserved medial crest fragment goes from the midshaft (the crest stops very abruptly at the midshaft break, indicating that it could be continued further proximally) to the base of the acrocoracoid, housing a canal for the tendon of the supracoracoid muscle, continuous to the supracoracoid groove; distally the crest curves and diminishes towards the acrocoracoid base (Fig. 5(B, C)). Such a morphology is observed in some enantiornithines from Dzharakuduk (i.e., specimens PO 4609, PO 4671, and PO 4825; Panteleev, 2018) unlike others from this locality (i.e., specimens PO 4819, PO 5203, and PO 6502) and *Piscivorenantiornis* (Wang et al., 2022a), which have a medial crest that terminates at the base of the scapular articular facet. A small and deep concavity is observed ventrally at midshaft in the boundary between the medial crest and the shaft, consistent with the presence of the incisure for the supracoracoid nerve (Fig. 5(B)), like the incisure observed in the enantiornithine *Longirostravis* (O'Connor, 2009). Instead this incisure, most enantiornithines present a supracoracoid nerve foramen piercing the shaft of the coracoid (Chiappe et al., 2007; Wang et al., 2016; Atterholt et al., 2018; Panteleev, 2018; Wang et al., 2022a).

The dorsal surface of the pterygoma is crushed and the medial margin is presumably eroded, given that the medial crest overhangs it. The laterosternal expansion of the pterygoma is thinner than the rest of the bone plate. The estimated ratio of the sternal width relative to the proximodistal length of the bone is low compared to other enantiornithines birds (0.33 in *I. romerali* LH-22; O'Connor, 2009). This ratio, which is very low in some Late Cretaceous taxa (Bufferaut, 1998) may appear wider in many slab specimens, exaggerated by crushing.

3.4. Furcula

The furcula is exposed in cranial view and has the typical Y-shaped observed in Enantiornithes (Chiappe and Witmer, 2002; O'Connor, 2022). The rami are broad and robust, becoming thinner towards the well-developed hypocleidium, the distal end of which is hidden under the radius (Fig. 6(A)). The distal third of the right ramus is broken and rotated (~60°) medially. Compared to the rest of the furcula, which is flattened, this fragment of the right ramus is three-dimensionally preserved, revealing the presence of the caudolateral groove (Fig. 5(B)) that is present in most enantiornithines. The caudal surface of the furcula is poorly preserved, but areas of high- and low-density bone can be discerned, with high-density areas distributed along the margins of the rami and in the dorsoventral axis of the hypocleidium (Fig. 6(B, C)). This configuration is confirmed by an analysis of density pattern (Fig. S1, Appendix A), and supports the presence of the caudolateral groove as well as a caudal keel on the hypocleidium, observed in some other enantiornithine taxa (Chiappe and Witmer, 2002; O'Connor, 2009; Atterholt et al., 2018; Wang et al., 2022a). A laterocaudally oriented facet in the omal end of the left ramus is observed, interpreted as the epicleidium and the scapular articular surface (Fig. 6). The complete morphology of the hypocleidium was recovered: a small 0.3 mm fragment was found under the radius, confirming that the hypocleidium did not continue much farther beyond its preserved length. With a length of 33% of the total ramus, *I. romerali* is within the range of other enantiornithines with "short" hypocleidia (e.g., *Concornis lacustris*) according to O'Connor (2009).

3.5. Humerus

The left humerus is flattened and exposed cranially (Fig. 7). The shaft is fractured in two places: near its midpoint and more proximally. The proximal epiphysis has been lost since the original description (Sanz et al., 1988), and only a small portion of the proximal fragment is currently preserved, although it is known that a well-developed deltopectoral crest and a short bicipital crest were

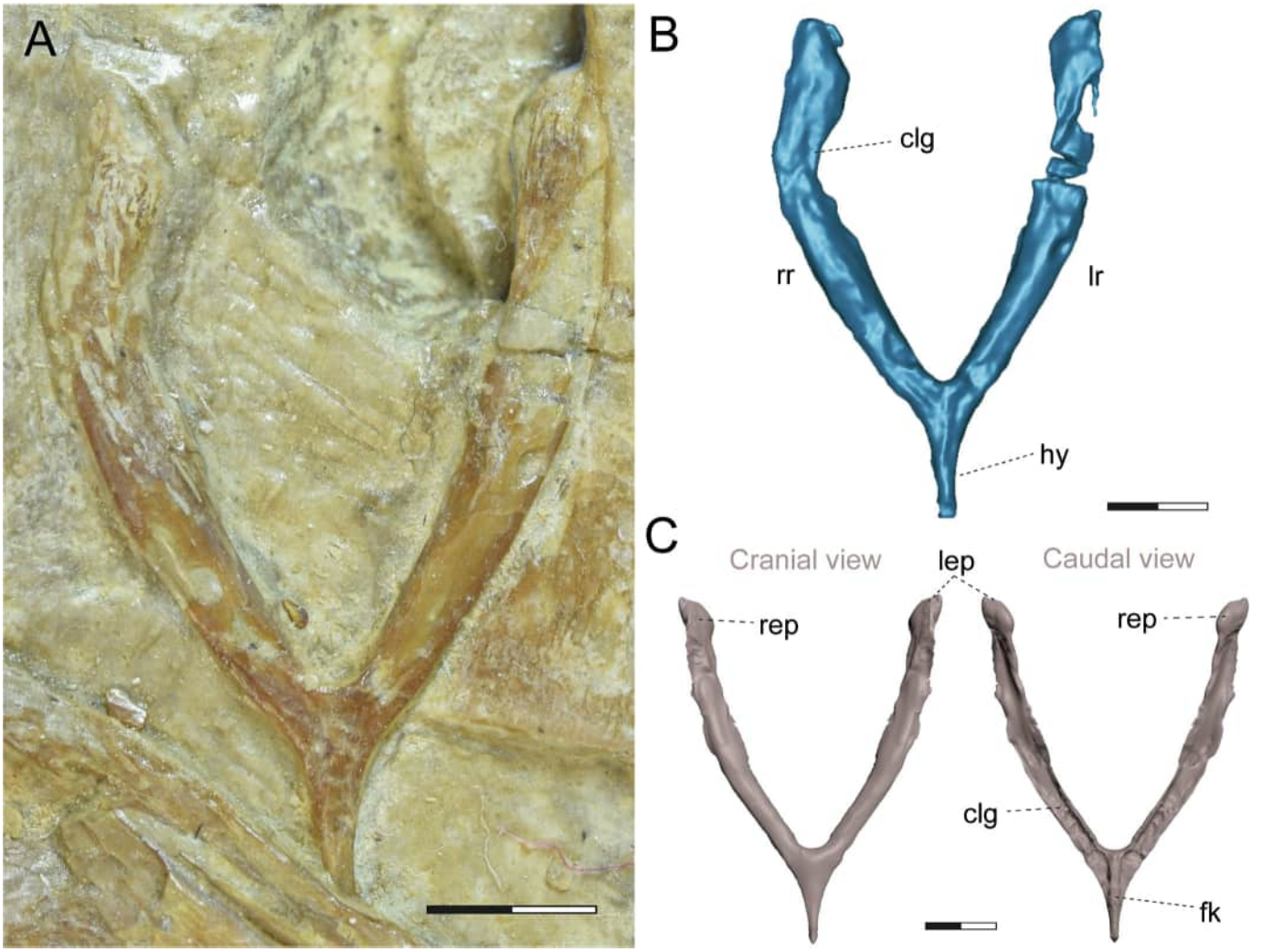

Fig. 6. Furcula of *Iberomesornis romerali*. **A.** Original fossil (holotype, LH-22). **B.** Virtual model segmented from micro-CT scan. **C.** Reconstructed model recovering the approximate furcular shape. Abbreviations: clg, caudolateral groove; fk, furcula keel; hy, hypocleidium; lep, left epicleidium; lr, left ramus; rep, right epicleidium; rr, right ramus. Scale bars: 2 mm.

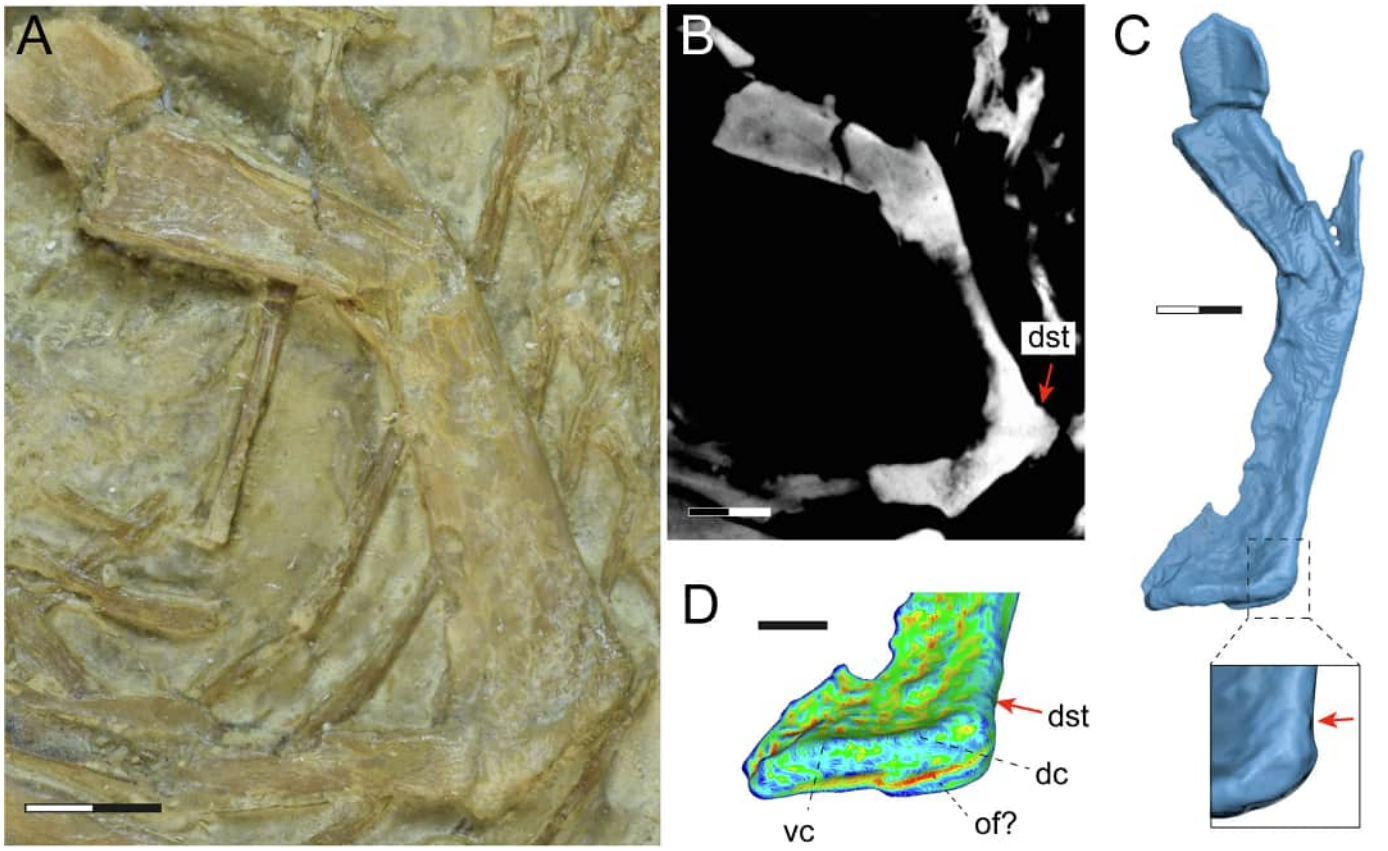

Fig. 7. Left humerus of *Iberomesornis romerali*. **A.** Original fossil (holotype, LH-22). **B.** Micro-CT slice of the whole humerus in cranial view. **C.** Virtual model segmented from micro-CT scan and detail of the dorso-distal edge showing the dorsal supracondylar tubercle. **D.** Segmented model of the distal humerus under topology filter. Abbreviations: dc, dorsal condyle; dst, dorsal supracondylar tubercle (red arrow); of, olecranon fossa; vc, ventral condyle. Scale bars: 2 mm (A-C), 1 mm (D).

present (Sereno, 2000; Sanz et al., 2002; Fig. S3, Appendix A). Micro-CT recovered new information about the distal humerus. The distal condyles are transversely oriented and weakly defined, having a 'strap-like' morphology contrasting with observations by Sereno (2000). The major axis of the ventral condyle appears longer than that of the dorsal condyle (Fig. 7(D)). In addition, a small dorsal supracondylar tubercle is identified at the dorsal margin of the distal epiphysis (Fig. 7(B–D)). This tubercle seems to be also present in *Eocathayornis* (Zhou, 2002) and *Cathayornis* (Zhou et al., 1992) from the Early Cretaceous, and it has been clearly identified in several enantiornithines from the Late Cretaceous (Chiappe et al., 2007; Walker et al., 2007; Lawver et al., 2011; Herrera et al., 2023). The dorsal supracondylar tubercle of *I. romerali* is more reminiscent to that of *Martinavis* (Walker et al., 2007) and MPEF-PV2359 (Lawver et al., 2011) than to the well-developed supracondylar process presented by *Yatenavis* (Herrera et al., 2023). A marked groove is observed in the distal view of the epiphysis, which may correspond to the olecranon fossa (Fig. 7(D)). This identification based on their topological location is tentative, given that the plastic behaviour of the bone during the taphonomic process has much flattened and deformed cranio-caudally the distal epiphysis.

4. Discussion

4.1. Phylogenetic affinity of Iberomesornis

The new CT data allows us to revise 13 morphological characters for *Iberomesornis* in the matrix from Atterholt et al. (2018): two from the caudal cervicals, three from the pygostyle, four from the coracoid, two from the furcula and two from the humerus (Table 2). In addition, we reinterpreted two other characters from the hindlimb. Despite the pygostyle is not fully fused, we considered the holotype of *I. romerali* as anatomically mature based on the fusion between the pubis and ischium and the absence of neurocentral sutures in the presacral vertebrae (Sanz et al., 2002; Griffin et al. 2021).

In the strict consensus tree of the first run of the analysis, Ornithothoraces formed a large polytomy. In the 50% majority tree, most Enantiornithes formed a large polytomy, with only subclades like the Bohaiornithidae, Pengornithidae, and Longipterygidae resolved (Fig. 8(A)). This likely reflects a combination of the unusual morphology of *Protopteryx*, which includes some 'ornithuromorph-like' traits such as the presence of a procoracoid process on the coracoid (Zhang and Zhou, 2000; Chiappe et al., 2020), and the fact that enantiornithine relationships are in general poorly resolved. Removing *Protopteryx* from the cladistic analysis produced a strict consensus tree with a topology that resolved Pengornithidae as the most basal clade of Enantiornithes (Fig. 8(B)). The position of *Iberomesornis* was consistently resolved as the outgroup to Longipterygidae, which agrees with a recent cladistic analysis that included two longipterygids, *Longirostravis* and *Rapaxavis* (see Wang et al., 2022b). The reconstruction of the pygostyle of *I. romerali* (Fig. 4) indicates it was 13% longer than the tarsometatarsus, which is consistent with other longipterygids which typically possess a proportionately large pygostyle (with the pygostyle exceeding the tarsometatarsus in length by 10% in *Rapaxavis* to 20% in *Longypteryx*; O'Connor, 2009). Such a derived

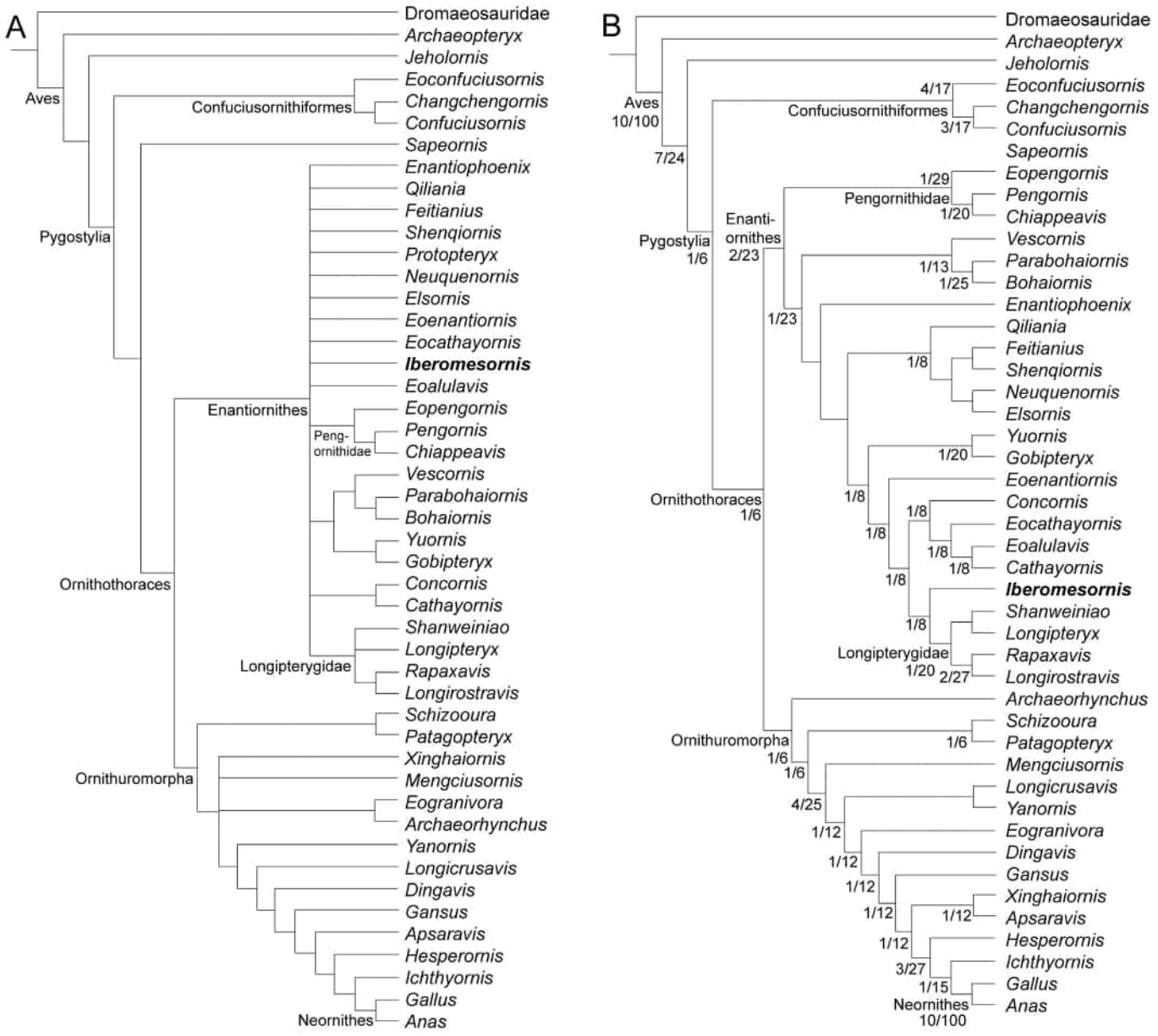

Fig. 8. Cladistic analyses of Aves using the new characters found in *Iberomesornis* from micro-CT data. **A.** Cladogram resulted from 50% majority rule including *Protopteryx*. **B.** Strict consensus single tree 923 steps long excluding *Protopteryx*, and displaying absolute and relative Bremer support values for nodes.

position close to Longipterygidae contrasts with the basal position previously recovered for *Iberomesornis* by Atterholt et al. (2018). The recognition of many classic enantiornithine morphologies like the ventrolateral processes of the pygostyle (Fig. 4), proximodistally aligned articular surfaces of the coracoid (Fig. 5), and caudolaterally excavated furcula (Fig. 6) have pushed this taxon further up in the tree.

4.2. Functional implications related to flight mechanics

Crown birds have two main muscles responsible for the wing movement, the mm. pectoralis and the supracoracoideus (SC), both having broad attachment originating on the sternum and its ventrally projecting keel (Raikow, 1985; Baumel and Witmer, 1993; Vanden Berge and Zweers, 1993; Biewener, 2011). The m. pectoralis inserts ventrally on the deltopectoral crest of the cranial surface of the proximal humerus, and depresses the wing producing the downstroke during flight. The tendon of SC passes through the triosseal canal – formed by the junction of the coracoid, scapula and furcula in the most of extant species – and inserts to the dorsal tubercle on the caudodorsal surface of the proximal humerus. With contraction, the SC acts as a pulley that elevates the wing (Raikow, 1985; Baumel and Witmer, 1993; Vanden Berge and Zweers, 1993; Biewener, 2011). This mechanism was presumably not present in the earliest birds like *Archaeopteryx*, *Sapeornis*, or *Confuciusornis*, which would have elevated their wings using dorsal musculature from the shoulder (Mayr, 2017; Pittman et al., 2022). However, *Sapeornis* could have had a partially enclosed tri-osseal canal similar to that of enantionithines, as proposed Wang et al. (2022a). The redirection and pulley action of the SC was an innovation that appeared close to the origin of Ornithothoraces, allowing a more efficient upstroke during flight. Within Ornithothoraces, the different contacts of the shoulder bones in Enantiornithes and Euornithes (the clade containing extant birds) may indicate a

different configuration of the SC pulley (Mayr, 2017; Novas et al., 2021; Wang et al., 2022a). For instance, unlike euornithines, most enantiornithines possess an elongated acromion of the scapula (which articulates distally with the epicleidium of the furcular ramus) and a less-developed acrocoracoid process, both suggesting that coracoid and furcula did not contact. *Iberomesornis* supports this interpretation as no areas of articulation between the epicleidium of the furcula and the coracoid were found in the segmented models (Figs. 5, 6). Based on this configuration present in numerous well-preserved enantiornithines, Mayr (2017) suggested that the SC tendon ran along the medial side of the acromion, rather than along the lateral side as in crown birds. The new CT data of the coracoid of *I. romerali* reveals a marked groove along the medial surface that indicates that SC tendon ran the coracoid medially from the midshaft to the tip of the acrocoracoid process (Fig. 5(B, C)). This character together with the absence of the procoracoid process in *I. romerali* is more consistent with the passage of the SC tendon through a partially enclosed triosseal canal by the lateral side of the acromion – although the scapula is not preserved –, similar to that reconstructed for the enantiornithine *Piscivorenantiornis inusitatus* (Wang et al., 2022a).

The lateralization of the scapular facet observed in *I. romerali* is noted to a lesser degree in *P. inusitatus* (Wang et al., 2022a); this configuration reduces the area for the glenoid facet of the coracoid. As the glenoid articulates with the humeral head, such a reduction might indicate a different range of motion of the wing among enantiornithines, although this interpretation is tentative since that the scapular glenoid is unknown due to the scapula is not preserved in *Iberomesornis*.

The fused clavicles (i.e., furcula) play a dynamic function in bird flight, with the rami bending laterally during the downstroke and medially during upstroke, working like a spring (Jenkins et al., 1988). Accordingly, the furcular shape correlates with flight performance in extant birds (Hui, 2002). 2D morphological analyses by Close and Rayfield (2012) found that the relatively narrow interclavicular angle of *Iberomesornis* and other enantiornithines was reminiscent of extant birds with continuous flapping flight. However, the cross-section of the rami seems point to a different stress-bearing. The presence of the caudolateral groove evidenced here in *Iberomesornis*, and also reported in other enantiornithes (Chiappe et al. 2007, named as dorsal furrow; Atterholt et al., 2018, named as dorsal groove; Wang et al., 2022a) implies a U-shaped cross-section of the rami, which is different from the oval section of modern birds. Such a different morphology indicates that the furcula of *Iberomesornis* and enantiornithines could support the mechanic stresses from the wing in a different way than neornithines, since that bone cross-section has high impact on the elasticity modulus, and hence, on the strength to deformation against stress (Hilderbrand and Gloslow, 2001). While this is predicted from beam theory, until our knowledge, the potential role of the cross-section of furcular rami has not been explored, and the functional effect of their different shape between enantiornithine and neornithine needs to be investigated in further research.

The geometry and shape of the humerus could provide functional information on birds' wings (De Margerie et al., 2005; Habib and Ruff, 2008; Serrano et al., 2020), but in *Iberomesornis*, the crushing of the bone and the loss of proximal epiphysis have precluded any functional interpretation. However, the identification of the dorsal supracondylar tubercle at the distal epiphysis (Fig. 7(B–D)) could provide some functional clue. This tubercle is the origin of the m. extensor carpi radialis, the muscle that connects the distal humerus with the proximal carpometacarpus in crown birds, conducting the extension of the wrist and, also contributing to the flexion of the elbow (Raikow, 1985; Baumel and Witmer, 1993; Vanden Berge and Zweers, 1993). A well-developed supracondylar dorsal tubercle was already present in Early Cretaceous ornithuromorphs (O'Connor et al., 2010), but its presence in Enantiornithes is less common. Among Late Cretaceous enantiornithines, *Yatenavis* has a prominent process (Herrera et al., 2023) while other taxa like *Martinavis*, *Elsornis* and MPEF-PV2359 present a less-prominent tubercle (Chiappe et al., 2007; Walker et al., 2007; Lawver et al., 2011), which is more similar with the tubercle identified in *Iberomesornis* (Fig. 7(B–D)). Apart from *Iberomesornis*, the dorsal supracondylar tubercle has been mentioned only to be present in two other enantiornitines from the Early Cretaceous: *Eocathayornis* and *Cathayornis* (Jin and Zhang, 1992; Zhou, 2002; Herrera et al., 2023). Interpolating from the wing mechanics of modern birds, the presence of the dorsal supracondylar tubercle suggests that *Iberomesornis* would have used elbow flexion and wrist extension frequently, as required during flapping flight in which the wings are flexed in the upstroke and spread in the downstroke (Raikow, 1985; Videler, 2006).

Iberomesornis romerali was smaller than *Eoalulavis hoyasi*, another enantiornithine described from Early Cretaceous of Las Hoyas. While body mass and other aerodynamic key parameters could be estimated for *Eoalulavis*, allowing to infer a capacity to perform powered flight through either continuous flapping or bounding (Serrano et al., 2018), the bone deformation in the holotype of *I. romerali* prevents an accurate estimate of body mass and wing area – crushed diaphysis results in overestimates of these parameters, which would result in aerodynamic reconstructions with a broad range of error (Serrano et al., 2015, 2017). However, we would expect that *I. romerali* had a capacity for powered flight similar to that inferred for *Eoalulavis* and other small enantiornithines (e.g., *Junornis*, *Protopteryx*, and *Orienantius*; Liu et al., 2019, 2017; Chiappe et al., 2020) given that the energetic demands of flight are lower in smaller birds, because as body mass increases, the power required for flapping flight increases more rapidly than the power available from the muscles (Pennycuick, 1969, 2008).

5. Conclusions

Micro-CT reconstruction of *Iberomesornis romerali* assessed in this study reveals new information regarding the anatomy and morphology of the cervical vertebrae, pygostyle, coracoids, furcula and humerus of this early bird. The new phylogenetic analyses support a derived position of *Iberomesornis* within Enantiornithes, close to Longypterygidae, rather than the basal position assigned by previous studies. The recognition of many classic enantiornithine morphologies like the ventrolateral processes of the pygostyle, proximodistally aligned articular surfaces of the coracoid, and dorsolaterally excavated furcula push this taxon further up in the tree.

From a functional point of view, the identification of (*i*) a well-developed groove for the passage of the main wing-elevator muscle (i.e., supracoracoideus) in the coracoid, and (*ii*) a dorsal supracondylar tubercle for insertion of a muscle responsible of wing flexion–extension (i.e., m. extensor carpi radialis) in the distal humerus, supports the capacity of *Iberomesornis* to perform some type of flapping flight. This capacity is consistent with other evidences previously reported, like 2D furcular shape (Close and Rayfield, 2012), the robust rami and long hypocleidium of the typical enantiornithine furcula (Chiappe and Witmer, 2002; Mayr 2017), or to have a smaller size than other enantiornithines (e.g., *Eoalulavis*) for which a full flapping capacity has been inferred (Serrano et al., 2018). However, the identification of the caudolateral groove conferring a U-shaped cross-section of the furcular rami in *Iberomesornis*, as in other enantiornithines, may indicate a different way for bearing the stress resulting from wing flapping with respect to flying neornithines.

Micro-CT also showed the coracoid's scapular facet of *I. romerali* opposite to the enantiornithine condition (i.e., concave vs. convex).

Although we cannot discard *I. romerali* acquired this ornithurine morphology independently, we conservatively attribute this morphology to deformation/crushing of the fossil. It is worth noting that while micro-CT scanning constitutes a powerful tool for the examination of fossils, a critical interpretation of the reconstructed structures and taphonomy is essential (Crane et al., 2025), particularly in fossils that are highly crushed. Further application of digital restoration techniques, including fixing breaks, mirroring, superimposing, repositioning and duplicating elements, and plastic retrodeformation (Lautenschlager, et al., 2016; Racicot, 2016; Pérez-Ramos and Figueirido, 2020; Herbst et al., 2022) could help to diminish the impact of taphonomical crushing and provide more robust 3D bone reconstructions of *Iberomesornis* and many other extinct birds, which promise to reveal even more about their anatomy and flight capabilities.

CRediT authorship contribution statement

Javier C. Terol: Writing – original draft, Visualization, Software, Methodology, Investigation, Formal analysis, Data curation, Conceptualization. **Alejandro Pérez-Ramos:** Writing – review & editing, Visualization, Validation, Software, Methodology, Investigation, Data curation. **Jingmai K. O'Connor:** Writing – review & editing, Visualization, Validation, Methodology, Formal analysis. **José Luis Sanz:** Writing – review & editing, Supervision, Investigation. **Francisco J. Serrano:** Writing – review & editing, Writing – original draft, Visualization, Validation, Supervision, Project administration, Investigation, Funding acquisition, Conceptualization.

Data availability

Data will be made available on request.

Declaration of competing interest

The authors declare that they have no known competing financial interests or personal relationships that could have appeared to influence the work reported in this paper.

Acknowledgements

We thank Mercedes Llandres and the Museo Paleontológico Castilla-La Mancha (Cuenca, Spain) for allowing scanning the holotype, and for providing high resolution pictures of *I. romerali*. We also thank Juan F. Pastor (Universidad de Valladolid) for providing skeletons of modern birds, Jesús Marugán (Universidad Autónoma de Madrid) and Marian Fregenal (Universidad Complutense de Madrid) for providing the maps and stratigraphic column used in Fig. 1. J.C.T. was awarded with a starting research grant (A1) to develop this study by the Universidad de Málaga (II Plan Propio de Investigación, Transferencia y Divulgación Científica). The study was funded by the Ministerio de Ciencia, Innovación y Universidades, projects PID2019-111185GB-100 (PI: Borja Figueirido) and CNS2023-145050 (PI: F.J.S.). Finally, thanks to the editors, Gilles Escarguel and Antoine Louchart, as well as to the reviewers, Michael Pitman and Jessie Atterholt, who have raised the level of this study considerably since the initial version.

Appendix A. Supplementary information

Supplementary information (including Figs. S1–S3) associated with this article can be found, in the online version, at: https://doi.org/10.1016/j.geobios.2024.11.006.

References

Abel, R., Laurini, C., Richter, M., 2012. A palaeobiologist's guide to "virtual" micro-CT preparation. Palaeontologia Electronica 15, 15.2.6T.
Atterholt, J., Hutchison, J.H., O'Connor, J.K., 2018. The most complete enantiornithine from North America and a phylogenetic analysis of the Avisauridae. PeerJ 6, e5910.
Baumel, J.J., King, A.S., Breazile, J.E., Evans, H.E., Vanden Berge, J.C., 1993. Handbook of Avian Anatomy: Nomina Anatomica Avium. Publication of the Nuttall Ornithological Club, Cambridge, Massachusetts.
Baumel, J.J., Witmer, L.M., 1993. Osteologia. In: Baumel, J.J., King, A.S., Breazile, J.E., Evans, H.E., Vanden Berge, J.C. (Eds.), Handbook of Avian Anatomy: Nomina Anatomica Avium. Club, Cambridge, Massachusetts, pp. 45–132.
Biewener, A.A., 2011. Muscle function in avian flight: achieving power and control. Philosophical Transactions of the Royal Society B: Biological Sciences 366, 1496–1506.
Britt, B.B., Makovicky, P.J., Gauthier, J., Bonde, N., 1998. Postcranial pneumatization in Archaeopteryx. Nature 395, 374–376.
Bufferaut, E., 1998. First evidence of enantiornithine birds from the Upper Cretaceous of Europe: postcranial bones from Cruzy (Hérault, southern France). Oryctos 1, 131–136.
Chiappe, L.M., 2002. Basal bird phylogeny: problems and solutions. In: Chiappe, L. M., Witmer, L.M. (Eds.), Mesozoic Birds: Above the Heads of Dinosaurs. University of California Press, Berjeley and Los Angeles, California, pp. 448–472.
Chiappe, L.M., Di, L., Serrano, F.J., Yuguang, Z., Meng, Q., 2020. Anatomy and flight performance of the early enantiornithine bird *Protopteryx fengningensis*: information from new specimens of the early cretaceous Huajiying formation of China. The Anatomical Record 303, 716–731.
Chiappe, L.M., Meng, Q., 2016. Birds of Stone: Chinese Avian Fossils from the Age of Dinosaurs. Johns Hopkins University Press, Baltimore, Maryland.
Chiappe, L.M., Suzuki, S., Dyke, G.J., Watabe, M., Tsogtbaatar, K., Barsbold, R., 2007. A new enantiornithine bird from the late cretaceous of the Gobi desert. Journal of Systematic Palaeontology 5, 193–208.
Chiappe, L.M., Walker, C.A., 2002. Skeletal Morphology and Systematics of the Cretaceous Euenantiornithes (Ornithothoraces: Enantiornithes). In: Chiappe, L. M., Witmer, L.M. (Eds.), Mesozoic Birds: Above the Heads of Dinosaurs. University of California Press, Berkeley and Los Angeles, California, pp. 240–267.
Chiappe, L.M., Witmer, L.M., 2002. Mesozoic Birds. Above the Head of Dinosaurs. University of California Press.
Close, R.A., Rayfield, E.J., 2012. Functional morphometric analysis of the Furcula in Mesozoic birds. PLoS One 7, e36664.
Crane, A., Benito, J., Chen, A., Musser, G., Torres, C.R., Clarke, J.A., Lautenschlager, S., Ksepka, D.T., Field, D.J., 2025. Taphonomic damage obfuscates interpretation of the retroarticular region of the *Asteriornis* mandible. Geobios 90, 31–43.
Cubo, J., Buscalioni, A.D., Legendre, L.J., Bourdon, E., Sanz, J.L., Ricqlès, A., 2022. Palaeohistological inferences of resting metabolic rates in *Concornis* and *Iberomesornis* (Enantiornithes, Ornithothoraces) from the Lower Cretaceous of Las Hoyas (Spain). Palaeontology 65, e12583.
De Margerie, E., Sanchez, S., Cubo, J., Castanet, J., 2005. Torsional resistance as a principal component of the structural design of long bones: comparative multivariate evidence in birds. The Anatomical Record 282A, 49–66.
Feo, T.J., Field, D.J., Prum, R.O., 2015. Barb geometry of asymmetrical feathers reveals a transitional morphology in the evolution of avian flight. Proceedings of the Royal Society B: Biological Sciences 282, 20142864.
Fregenal-Martínez, M., Nieves Meléndez, N., Muñoz-García, M.B., Elez, J., Horra, R.D., 2017. The stratigraphic record of the Late Jurassic-Early Cretaceous rifting in the Alto Tajo-Serranía de Cuenca region (Iberian Ranges, Spain). Revista de la Sociedad Geológica de España 30, 113–142.
Goloboff, P.A., Morales, M.E., 2023. TNT version 1.6, with a graphical interface for MacOS and Linux, including new routines in parallel. Cladistics 39, 144–153.
Grau, J.F.P., 2003. Técnicas de análisis de imagen: Aplicaciones en Biología. Universitat de València.
Habib, M.B., Ruff, C.B., 2008. The effects of locomotion on the structural characteristics of avian limb bones. Zoological Journal of the Linnean Society 153, 601–624.
Herbst, E.C., Meade, L.E., Lautenschlager, S., Fioritti, N., Scheyer, T.M., 2022. A toolbox for the retrodeformation and muscle reconstruction of fossil specimens in Blender. Royal Society Open Science 9, 220519.
Herrera, G.Á., Agnolín, F., Rozadilla, S., Lo Coco, G.E., Manabe, M., Tsuihiji, T., Novas, F.E., 2023. New enantiornithine bird from the uppermost Cretaceous (Maastrichtian) of southern Patagonia, Argentina. Cretaceous Research 144, 105452.
Hilderbrand, M., Gloslow Jr., G.E., 2001. Analysis of Vertebrate Structure. John Wiley & Sons Ed.
Hu, H., O'Connor, J.K., 2017. First species of Enantiornithes from Sihedang elucidates skeletal development in Early Cretaceous enantiornithines. Journal of Systematic Palaeontology 15, 909–926.
Hui, C.A., 2002. Avian furcula morphology may indicate relationships of flight requirements among birds. Journal of Morphology 251, 284–293.
Jenkins, F.A., Dial, K.P., Goslow, G.E., 1988. A cineradiographic analysis of bird flight: the wishbone in starlings is a spring. Science 241, 1495–1498.
Jin, E., Zhang, J., 1992. Preliminary report on a Mesozoic bird from Liaoning, China. Chinese Science Bulletin 37, 1365–1368.
Knoll, F., Chiappe, L.M., Sanchez, S., Garwood, R.J., Edwards, N.P., Wogelius, R.A., Sellers, W.I., Manning, P.L., Ortega, F., Serrano, F.J., Marugán-Lobón, J., Cuesta, E.,

Escaso, Sanz, J.L., . A diminutive perinate European Enantiornithes reveals an asynchronous ossification pattern in early birds. Nature Communications 9, 937.
Kurochkin, E.N., 1985. A true carinate bird from lower Cretaceous deposits in Mongolia and other evidence of early Cretaceous birds in Asia. Cretaceous Research 6, 271–278.
Lawver, D.R., Debee, A.M., Clarke, J.A., Rougier, G.W., 2011. A New Enantiornithine Bird from the Upper Cretaceous La Colonia Formation of Patagonia, Argentina. Annals of Carnegie Museum 80, 35–42.
Liu, D., Chiappe, L.M., Serrano, F., Habib, M., Zhang, Y., Meng, Q., 2017. Flight aerodynamics in enantiornithines: information from a new Chinese Early Cretaceous bird. PLoS ONE 12, e0184637.
Liu, D., Chiappe, L.M., Zhang, Y., Serrano, F.J., Meng, Q., 2019. Soft tissue preservation in two new enantiornithine specimens (Aves) from the Lower Cretaceous Huajiying Formation of Hebei Province, China. Cretaceous Research 95, 191–207.
Mayr, G., 2017. Pectoral girdle morphology of Mesozoic birds and the evolution of the avian supracoracoideus muscle. Journal of Ornithology 158, 859–867.
Navalón, G., Marugán-Lobón, J., Chiappe, L.M., Luis Sanz, J., Buscalioni, Á.D., 2015. Soft-tissue and dermal arrangement in the wing of an Early Cretaceous bird: implications for the evolution of avian flight. Scientific Reports 5, 14864.
Nebreda, S.M., Chiappe, L.M., Navalon, G., Chinsamy, A., Sanz, J.L., Buscalioni, A.D., Marugán-Lobón, J., 2023. A new enantiornithine specimen from the Lower Cretaceous of Las Hoyas: avifaunal diversity and life-history of a wetland Mesozoic bird. Spanish Journal of Palaeontology 38, 1–13.
Novas, F.E., Agnolin, F.L., Ezcurra, M.D., Temp Müller, R., Martinelli, A.G., Langer, M. C., 2021. Review of the fossil record of early dinosaurs from South America, and its phylogenetic implications. Journal of South American Earth Science 110, 103341.
O'Connor, J.K., 2009. A systematic review of the Enantiornithes (Aves: Ornithothoraces). University of Southern California.
O'Connor, J., 2022. Enantiornithes. Current Biology 32, R1166–R1172.
O'Connor, J., Chiappe, L.M., Bell, A., 2011. Pre-modern birds: avian divergences in the mesozoic. In: Dyke, G., Kaiser, G. (Eds.), Living Dinosaurs. The Evolutionary History of Modern Birds, Wiley-Blackwell, Oxford, UK, pp. 39–116.
O'Connor, J.K., Gao, K.-Q., Chiappe, L.M., 2010. A new ornithuromorph (Aves: Ornithothoraces) bird from the Jehol Group indicative of higher-level diversity. Journal of Vertebrate Paleontology 30, 311–321.
O'Connor, J.K., Zhang, Y., Chiappe, L.M., Meng, Q., Quanguo, L., Di, L., 2013. A new enantiornithine from the Yixian Formation with the first recognized avian enamel specialization. Journal of Vertebrate Paleontology 33, 1–12.
O'Connor, J.K., Zhou, Z., 2013. A redescription of *Chaoyangia beishanensis* (Aves) and a comprehensive phylogeny of Mesozoic birds. Journal of Systematic Palaeontology 11, 889–906.
Panteleev, A.V., 2018. Morphology of the Coracoid of Late Cretaceous Enantiornithines (Aves: Enantiornithes) from Dzharakuduk (Uzbekistan). Paleontological Journal 52, 201–207.
Pei, R., Pittman, M., Goloboff, P.A., Dececchi, T.A., Habib, M.B., Kaye, T.G., Larsson, H. C.E., Norell, M.A., Brusatte, S.L., Xu, X., 2020. Potential for powered flight neared by most close Avialan relatives, but few crossed its thresholds. Current Biology 30, 4033–4046.e8.
Pennycuick, C.J., 1969. The mechanics of bird migration. Ibis 111, 525–556.
Pennycuick, C.J., 2008. Modelling the flying bird. AP Theoretical Ecology Series. Elsevier, Academic Press, Oxford.
Pérez-Ramos, A., Figueirido, B., 2020. Toward an "ancient" virtual world: improvement methods on X-ray CT data processing and virtual reconstruction of fossil skulls. Frontiers in Earth Science 8, 345.
Pittman, M., Kaye, T.G., Wang, X., Zheng, X., Alexander Dececchi, T., Hartman, S.A., 2022. Preserved soft anatomy confirms shoulder-powered upstroke of early theropod flyers, reveals enhanced early pygostylian upstroke, and explains early sternum loss. Proceedings of the National Academy of Sciences of the USA 119, e2205476119.
Poyato-Ariza, F.J., Buscalioni, A.D. (Eds.), 2016. Las Hoyas: a Cretaceous Wetland: a Multidisciplinary Synthesis after 25 Years of Research on an Exceptional Fossil Lagerstatte from Spain. Verlag Dr. Friedrich Pfeil, Munich, p. 262.
Raikow, R.J., 1985. Locomotor system. In: Form and Function in Birds, pp. 57–147.
Sanz, J.L., Bonaparte, J.F., 1992. *Iberomesornis romerali*, a fossil small bird articulated skeleton from the Early Cretaceous of Spain. Proceedings of the II International Symposium on Avian Paleontology, Los Angeles 1988, 39–49.
Sanz, J.L., Bonaparte, J.F., Lacasa, A., 1988. Unusual Early Cretaceous birds from Spain. Nature 331, 433–435.
Sanz, J.L., Buscalioni, A.D., 1992. A new bird from the Early Cretaceous of Las Hoyas, Spain, and the early radiation of birds. Paleontology 35, 829–845.
Sanz, J.L., Chiappe, L.M., Pérez-Moreno, B.P., Buscalioni, A.D., Moratalla, J.J., Ortega, F., Poyato-Ariza, F.J., 1996. An Early Cretaceous bird from Spain and its implications for the evolution of avian flight. Nature 382, 442–445.
Sanz, J.L., Pérez-Moreno, B.P., Chiappe, L.M., Buscalioni, Á.D., 2002. The Birds from the Lower Cretaceous of Las Hoyas (Province of Cuenca, Spain). In: Chiappe, L. M., Witmer, L.M. (Eds.), Mesozoic Birds: above the Heads of Dinosaurs. University of California Press, pp. 209–229.
Schindelin, J., Arganda-Carreras, I., Frise, E., Kaynig, V., Longair, M., Pietzsch, T., Preibisch, S., Rueden, C., Saalfeld, S., Schmid, B., Tinevez, J.-Y., White, D.J., Hartenstein, V., Eliceiri, K., Tomancak, P., Cardona, A., 2012. Fiji: an open-source platform for biological-image analysis. Nature Methods 9, 676–682.
Sereno, P.C., 2000. *Iberomesornis romerali* (Aves, Ornithothoraces) reevaluated as an Early Cretaceous enantiornithine. Neues Jahrbuch für Geolgie and Paläontolgie Abhandlungen 215, 365–395.
Serrano, F.J., Chiappe, L.M., Palmqvist, P., Figueirido, B., Marugán-Lobón, J., Sanz, J.L., 2018. Flight reconstruction of two European enantiornithines (Aves, Pygostylia) and the achievement of bounding flight in Early Cretaceous birds. Palaeontology 61, 359–368.
Serrano, F.J., Costa-Pérez, M., Navalón, G., Martín-Serra, A., 2020. Morphological disparity of the humerus in modern birds. Diversity 12, 173.
Sutton, M.D., Rahman, I.A., Garwood, R.J., 2014. Techniques for Virtual Palaeontology. Wiley Blackwell.
Vanden Berge, J.C., Zweers, G.A., 1993. Myologia. In: Handbook of Avian Anatomy: Nomina Anatomica Avium. Publications of the Nuttall Ornithological Club (USA).
Voeten, D.F.A.E., Cubo, J., De Margerie, E., Röper, M., Beyrand, V., Bureš, S., Tafforeau, P., Sanchez, S., 2018. Wing bone geometry reveals active flight in *Archaeopteryx*. Nature Communications 9, 923.
Walker, C.A., Buffetaut, E., Dyke, G.J., 2007. Large euenantiornithine birds from the Cretaceous of southern France, North America and Argentina. Geological Magazine 144, 977–986.
Wang, M., 2023. A new specimen of *Parabohaiornis martini* (Avialae: Enantiornithes) sheds light on early avian skull evolution. Vertebrata PalAsiatica 61, 90–107.
Wang, X., Cau, A., Luo, X., Kundrát, M., Wu, W., Ju, S., Guo, Z., Liu, Y., Ji, Q., 2022b. A new bohaiornithid-like bird from the Lower Cretaceous of China fills a gap in enantiornithine disparity. Journal of Paleontology 96, 961–976.
Wang, S., Ma, Y., Wu, Q., Wang, M., Hu, D., Sullivan, C., Xu, X., 2022a. Digital restoration of the pectoral girdles of two Early Cretaceous birds and implications for early-flight evolution. Elife 11, e76086.
Wang, M., Zhou, Z., 2020. Anatomy of a new specimen of *Piscivorenantiornis inusitatus* (Aves: Enantiornithes) from the Lower Cretaceous Jehol Biota. Journal of Vertebrate Paleontology 40, e1783278.
Zhang, F., Zhou, Z., 2000. A primitive enantiornithine bird and the origin of feathers. Science 290, 1955–1959.
Zhou, Z., 2002. A new and primitive enantiornithine bird from the Early Cretaceous of China. Journal of Vertebrate Paleontology 22, 49–57.